ELSEVIER

Biomaterials 22 (2001) 269–279

Biomaterials

Corrosion behavior of a welded stainless-steel orthopedic implant

L. Reclaru[a,*], R. Lerf[b], P.-Y. Eschler[a], J.-M. Meyer[c]

[a]PX. Tech, Blvd des Eplatures 46, 2304 La Chaux-de-Fonds, Switzerland
[b]STRATEC Medical, Eimattstr. 3, 4436 Oberdorf, Switzerland
[c]School of Dentistry, University of Geneva, 19 Rue Barthelemy-Menn, 1205 Geneva, Switzerland

Received 13 January 1999; accepted 10 May 2000

Abstract

The corrosion behavior of combinations of materials used in an orthopedic implant: the spherical part (forged or forged and annealed) constituting the head, the weld (tungsten inert gas (TIG) or electron beam (EB) techniques), and the cylindrical part (annealed) constituting the shaft of a femoral prosthesis – has been investigated. Open-circuit potentials, potentiodynamic curves, Tafel slope, mixed potential theory and susceptibility to intergranular attack are electrochemical and chemical procedures selected for this work. Electrochemical measurements using a microelectrode have been made in the following zones: spherical part, cylindrical part, weld, and weld/sphere, and weld/shaft interfaces. To detect intergranular attack, the Strauss test has been used. At the interfaces, corrosion currents, measured (I_{corr}) and predicted (I_{couple}) are low, in the order of the pico- to nanoampere. The electrochemical behavior of the electron beam (EB) weld is better than that of the tungsten inert gas (TIG). Welds at interfaces can behave either anodically or cathodically. It is better if welds, which are sensitive parts of the femoral prosthesis, behave cathodically. In this way, the risk of starting localized corrosion (pitting, crevice or intergranular corrosion) from a galvanic couple, remains low. From this point of view, the sample with the EB weld offers the best behavior. All the other samples containing a TIG type of weld exhibit a less favorable behavior. The mechanical treatments (forged, and forged and annealed) of the steel sphere did not show any difference in the corrosion behavior. No intergranular corrosion has been observed at the weld/steel interface for unsensitized samples. With sensitized samples, however, a TIG sample has exhibited some localized intergranular corrosion at a distance of 500 μm along the weld/stainless steel (sphere) interface.

Keywords: Microelectrode; Electrochemical microcell; Microelectrochemistry; Galvanic corrosion; Intergranular attack; Strauss test; Welding; Electron beam technique; Tungsten inert gas technique; Stainless steels; Orthopedic prostheses

1. Introduction

Certain types of orthopedic implants such as monobloc hip stems are often made of two elements welded together. The reasons for doing such joining are rather technical or commercial in nature than based on a clinical demand. Welding may reduce the cost of manufacturing the implants and makes production more easy. Welding together two different parts leads to the selection of materials more adequate to the function of the said part. E.g. in monobloc hip implants, the stem part may be manufactured out of low-carbon, high-strength forged CoCrMo alloy and the head part out of high-carbon, cast and wear-resistant CoCrMo alloy.

Nevertheless, welds are recognized as zones which are particularly sensitive to corrosion [1,2]. The in vitro corrosion tests usually selected for this type of system are tests for fretting corrosion [3–11], or fatigue and stress corrosion tests [12–17], as well as the analysis of the metallic cations released in synthetic physiological solutions [4–6,11,18]. In vivo investigations on the corrosion resistance and analyses of released metallic ions have also been performed on prosthetic systems [19–22]. In a welded system, the weld itself often represents a corrosion-prone area. Welding operations affect the properties of the weld and of the adjacent alloy. This includes microsegregation, precipitation of secondary phases, formation of unmixed zones, recrystallization and grain growth in the weld heat-affected zone (HAZ), volatilization of alloying elements from the molten weld pool and contamination of the solidifying weld pool [1]. It is often difficult to determine why welds corrode. Several factors are involved, like weldment design, fabrication technique,

* Corresponding author. Tel.: +41-32-924-02-90; fax: +41-32-924-01-41.
E-mail address: lucien.reclaru@groupepx.com (L. Reclaru).

0142-9612/01/$ - see front matter
PII: S0142-9612(00)00185-X

weldment practice, weldment sequence, moisture contamination, organic or inorganic contamination, oxide film and scale, weld slag and spatter, incomplete weld penetration or fusion, porosity, cracks (crevices), high residual stresses, improper choice of filler metal, final surface finish, etc. [1].

The clinical consequences of at least partially corroding implants are well known: Release of solutes, i.e. the corrosion products, at an implant site may cause histological changes in the local tissue by either direct toxic effects or a local hypersensitivity reaction, since elemental nickel, cobalt and chrome as well as their compounds are known allergens. This adverse biological response of the tissue surrounding the implant may for example cause loosening of a part of joint replacement and lead to a revision surgery of the said orthopedic implant. On the other hand, it cannot be assumed that all the released material or ions will remain permanently localized to the implant site. Dissolved metals can gain access to the blood stream with the possibility of distant toxic effects [23–30]. However, a thorough literature search was not able to produce any reference on the specific corrosion behavior of welds in orthopedic implants. Therefore, it has been decided to investigate the effects of two types of well-known and commercially used welding systems, to select the least offensive one for orthopedic applications.

In the present study, a model orthopedic system was studied. The system was composed of the following: cylindrical part/weld/spherical part. Such a construct mimics the joining of the neck of a femoral stem to the femoral head part. In the orthopedic field, the use of the so-called REX 734 stainless steel (X4CrNiMnMoNbN 21-9-5-2) becomes more widespread. The interest of the REX 734 type steel is based on the following facts:

- high strength, even in the annealed conditions;
- high work hardening rate, i.e. large strength potential for work-hardened semi-products;
- high corrosion resistance;
- competitive price.

On the other hand, due to its high nitrogen content, the machining of REX 734 type material is far from being easy. Consequently, welding this stainless steel to minimize machining operations may become commercially attractive. On this background, a basic study on the corrosion of welds in REX 734 implant steel was initiated. Mainly, the interfaces weld/stainless steel obtained with different welding techniques will be studied: electron beam and tungsten inert gas. The microelectrode technique will be applied.

The microelectrode technique allows the acquisition of information related to the electrochemical behavior of welding interfaces in a "real" orthopedic system, and thus allows to compare with results obtained from prediction techniques.

In the orthopedic prostheses field, the use of the so-called REX 734 stainless steel for load-bearing implants is becoming widespread. The interest of the REX 734 type steel is based on the following facts:

- growing use of REX 734 type steel (X4CrNiMnMoNbN 21-9-5-2) for orthopedic implants;
- importance of the joining for certain types of implants (e.g. Monobloc hip stems, spine systems, etc.);
- investigation of welding as a joining method for REX 734.

2. Materials and methods

For the sake of simplicity, the weld joined a cylindrical and a spherical (conical) part, representing approximately the shape of a femoral prosthesis. The diameter of the samples at the weld was about 42 mm, giving rise to a length of the weld of about 132 mm. Two types of welding methods have been used:

- electron beam welding (EB, in vacuo, fully automatic, without any filler metal);
- tungsten inert gas (TIG, in protective atmosphere, semi-automatic welding devices, filler metal standard 1.4316).

The cylindrical parts were machined out of commercial semi-products in the annealed (recrystallized) conditions. Two different metallurgical conditions are performed for the spherical (conical) part: (a) forged and (b) forged and annealed at 1050°C for 1 h with the water quench treatment.

The nominal composition (wt%) of the REX 734 type steel is shown in Table 1.

For the cylindrical parts, two different lots of REX 734 d from the same supplier have been used; lot A and lot B. The two types of welding and two metallurgical treatments therefore led to four orthopedic system combinations (Table 2).

2.1. Specimens

Two transversal and two longitudinal sections have been made to obtain four identical samples (Figs. 1 and 2).

Table 1
Nominal composition of the REX 734 type implant steel

Composition (wt%)	C	Cr	Ni	Mn	Mo	Nb	N
	< 0.06	21.00	9.00	4.00	2.20		0.40

Table 2
Combination of materials used in orthopedic implants

Code orthopedic system	Materials		
	Spherical part	Weld	Cylindrical part
1	Forged	EB	Annealed (A)
2	Forged	TIG	Annealed (B)
3	Forged and annealed	EB	Annealed (A)
4	Forged and annealed	TIG	Annealed (B)

Fig. 1. Schematic presentation of sample preparation.

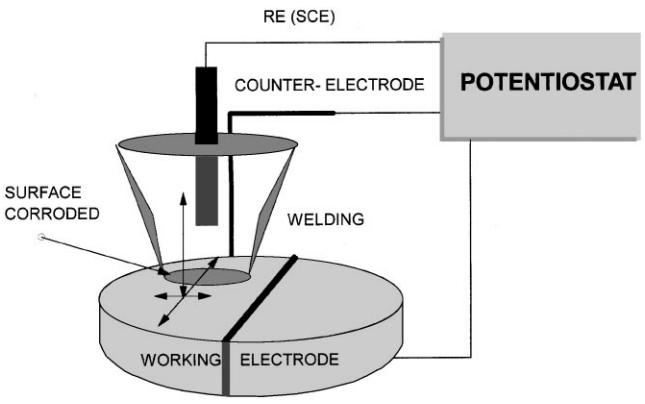

Fig. 2. Experimental setup with the electrochemical microcell.

For the corrosion tests using the microelectrode technique, a sample has been embedded through the welding site, and polished with 1 μm diamond paste.

To evaluate the corrosion resistance of the system weld/stainless steel, two corrosion tests were performed.

2.2. Microelectrode technique

Experimental setup with the electrochemical microcell: In order to perform corrosion tests within the range of 1 μm, it is necessary to reduce the surface area of the sample. In general, two techniques are available:

(a) the first possibility is to use a mounted wire. The disadvantage of this technique is that wires can be obtained only from a few commercial steels;
(b) the second possibility is to cover part of sample's surface with a protective lacquer (photolacquer). The disadvantage of this technique is the possible detachment of the lacquer in cathodic polarization and only one measurement per sample is possible.

Because of the above-mentioned problems, the size of electrochemical cell itself has been modified. Fig. 3 shows the experimental setup with the electrochemical microcell used. It is made of a truncated conical electrochemical cell with a capacity of 0.7 ml. The opening in the measuring area is 400 μm in diameter. The reference electrode is a saturated calomel microelectrode (SCE), obtained from Microelectodes, Inc., Londonderry, New Hampshire, USA. It is placed at a distance of 4 mm from the surface of the working electrode. The counter-electrode is made of a platinum wire. The working electrode is the embedded sample, connected to a differential electrometer. The microcell is thus moved along the polished surface of the sample, to perform the various electrochemical measurements. The system used allows a displacement of the electrochemical microcell along three orthogonal axes. The whole electrochemical setup has been placed in a Faraday cage, and was controlled by an EG&G Par model 273A potentiostat, which has been modified according to the manufacturer's instructions for a 1 nA current range and 10 pA current noise. A quite similar system has been used by Böhni et al. [31–33].

Testing medium: NaCl 0.1 M solution.

Electrochemical parameters: Electrochemical parameters investigated were as follows:

- open-circuit potential (E_{oc}) for 1 h period;
- potentiodynamic polarization curves from 250 mV versus E_{oc} to 500 mV;
- Tafel slopes and calculation of the corrosion currents;
- application of mixed potential theory.

Measurements have been made in the spherical part (stainless steel), in the cylindrical part (stainless steel), in the weld, and at the interfaces weld/cylindrical part, and weld/spherical part (Fig. 3). Potential scanning for the potentiodynamic polarization curves in the anodic zone has been limited up to 500 mV to avoid gas evolution (oxygen), which, in a capillary system, could possibly stop the current flow or increase the resistance in the electrolyte (IR).

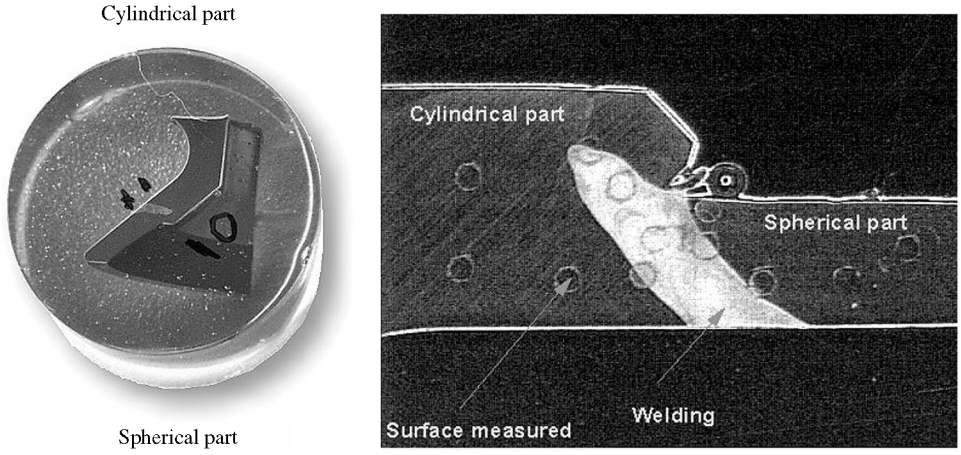

Fig. 3. Topography of the measurement zones in sample #1; stainless steel stem zone; stainless steel sphere zone; welding zone.

Interfaces form galvanic assemblies (a pair of dissimilar conductors, commonly metals, in electrical contact). Therefore, the electrochemical values E_{corr} and I_{corr} as measured at the interfaces can be added to the values of galvanic couples (E_{couple} and I_{couple}).

For the measurements at the interfaces, the microelectrode has always been placed so that half of the surface was on each side of the interface. Therefore, the ratio of the surfaces for the galvanic couples has always been equal to 1.

2.3. Intergranular test, Strauss method

Another type of corrosion may develop in the case of welds: intergranular corrosion [1,2]. The behavior of welds in intergranular corrosion has also been investigated using the Strauss method, according to *ASTM A 262-90, Practice F* [34]. For each orthopedic system combination, three samples have been tested (Fig. 2): two of them have been sensitized by a thermal treatment (680°C for 1 h), and one was not. Particular attention has been paid to the interfaces weld/stem and weld/sphere, since these zones are usually prone to intergranular corrosion because of the structural perturbations.

Testing conditions: 120 h at boiling temperature in a medium containing copper sulfate–metallic copper–sulfuric acid at 50% (236 ml H_2SO_4, 72 g $CuSO_4 \cdot 5H_2O$, 110 g metallic copper and 400 ml distilled water). After the test, samples are rinsed in deionized water, washed in diluted nitric acid, rinsed again in deionized water, and dried. Samples have been observed with low-power optical microscopy, and with scanning electron microscopy.

2.4. Surface analysis

Some of the corroded zones of samples were observed by scanning electron microscopy (SEM). A JEOL JSM 6300 instrument with an energy diffraction X-ray (EDX) (Link Isis) microprobe was used.

3. Results and discussion

The specific microstructures of the welds are generated by the welding technique parameters. This effect has not been studied specifically, and the usual parameters of each technique have been used, without attempting to correlate welding parameters with electrochemical behavior. However, changes in susceptibility to corrosion have been observed among samples from the two welding techniques, as described below.

3.1. Electrochemical investigation

3.3.1. The potentiodynamic polarization curves

Three polarization curves have been traced for each sample in the parts stainless steel stem, stainless steel sphere, welding, and the interfaces welding/stem and welding/sphere. A mean of these measured potentiodynamic polarization curves has then been calculated.

These mean polarization curves for welds EB #1, TIG #2, EB #3 and TIG #4 are shown in Fig. 4.

For the stainless steel parts, mean polarization curves have been calculated for identical elements as shown in Table 2. Thus, a unique curve has been established from the three measured curves for stainless steel sphere, forged, samples #1 and #2 (6 curves in total, grouped in a unique mean curve). Then, similarly, forged and annealed stainless steel sphere, samples #3 and #4, stainless steel stem Batch A from samples #1 and #3, and, stainless steel stem Batch B from samples #2 and #4. The curves resulting from these groupings are shown in Fig. 5.

The values of the corrosion current I_{corr} and corrosion potential E_{corr}, and the Tafel slopes calculated from the polarization curves, are shown in Table 3.

From those results, welds of the EB type exhibit a better electrochemical behavior than those made using the TIG welding system. Values of I_{corr} are within the range of several hundreds of picoamperes for EB welds, and in the nanoamperes range for the TIG welds. EB welding of sample #1 exhibits the best behavior.

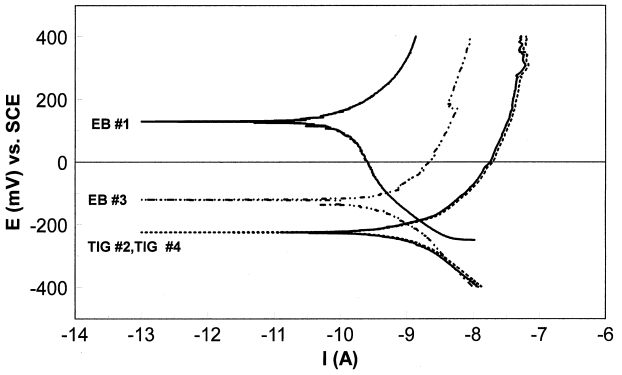

Fig. 4. Mean potentiodynamic polarization curves for welds EB #1, TIG #2, EB #3 and TIG #4.

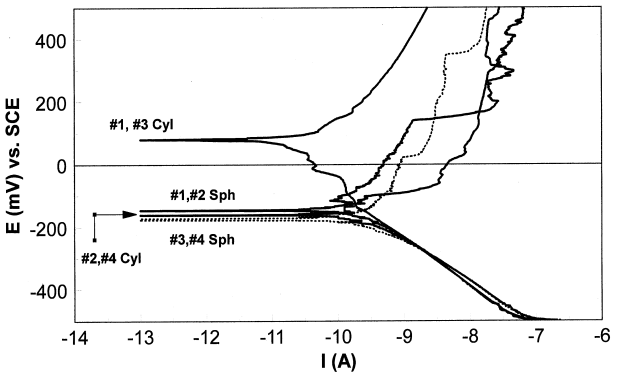

Fig. 5. Potentiodynamic polarization curves as measured on stainless steel (stem and sphere). Mean value of the measured curves on stem samples #1, #3 (Cyl), on stem samples #2, #4 (Cyl), on sphere samples #1, #2 (Sph), and on sphere samples #3, #4 (Sph).

Considering the calculated values for I_{corr} (Table 3), stainless steel samples show a better behavior than the weldings. From an electrochemical point of view, there is no visible difference among the stainless steel sphere samples prepared with different mechanical treatments (forged versus forged and annealed). However, steel from Batch A used to make the stem part of samples #1 and #3 has a better electrochemical behavior than the one from Batch B used to make the other stem samples. The E_{corr} value is in the cathodic range at + 30 mV, and the I_{corr} value is 61 pA.

Another comparative analysis can be made about the behavior of the interfaces weld/stainless steel. In Figs. 6–9, mean polarization curves for the interfaces weld/stem, weld/sphere, and weld of each sample are presented.

It is interesting to compare the I_{corr} and E_{cor} values measured from the potentiodynamic polarization curves traced at the interfaces, with the values predicted from the mixed potential theory (Table 4).

3.3.2. The predicted current and potential after the mixed potential theory

The direct measurement of galvanic couples provides information on the intensity of galvanic currents. However, to better understand the specific kinetic parameters of the galvanic cell, the prediction methods were also examined. In addition, in this case, several different methods were taken into consideration: Evans' plot, application of the mixed potential theory, plot intercepts from potentiodynamic polarization curves, and so forth. For the purpose of this study, the mixed potential theory was selected.

Galvanic corrosion of alloys treated by the application of the mixed potential theory was first described by Wagner and Traub [35]. The theory is based on two simple hypotheses: (1) any electrochemical reaction can

Table 3
Electrochemical parameters calculated from polarization curves

Place of measure		Code	E_{corr} (mV)	I_{corr} (pA)	α_c (mV)	$\lvert\beta_a\rvert$ (mV)
Weld	EB	#1	+ 130	491	75	186
	EB	#3	− 131	808	270	242
	TIG	#2	− 235	2191	236	202
	TIG	#4	− 227	2190	221	268
Cylindrical part	Annealed A	#1, #3	+ 30	61	147	235
	Annealed B	#2, #4	− 148	181	217	152
Spherical part	Forged and annealed	#1, #2	− 140	166	287	108
	Forged	#3, #4	− 168	218	235	115

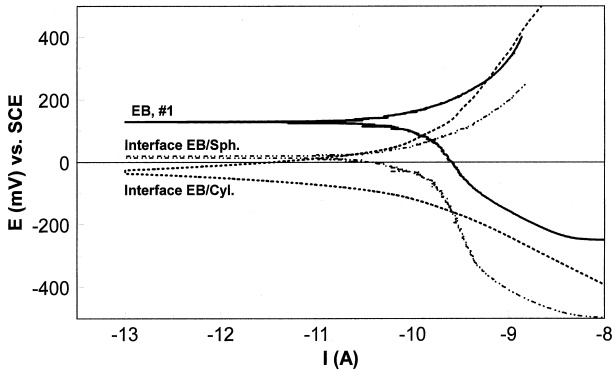

Fig. 6. Means of the potentiodynamic polarization curves measured from sample #1; weld EB #1; interface weld EB/cylindrical part; interface weld EB/spherical part.

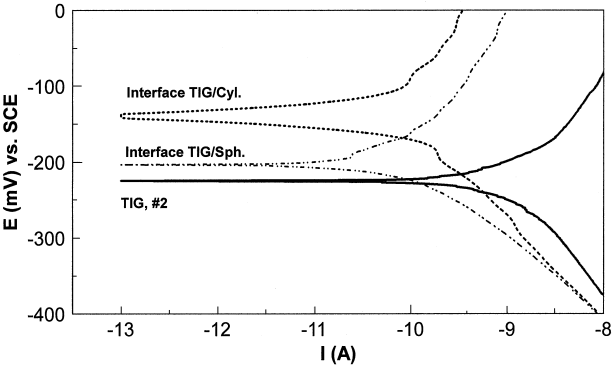

Fig. 7. Means of the potentiodynamic polarization curves measured from sample #2; weld TIG #2; interface weld TIG/cylindrical part; interface weld TIG/spherical part.

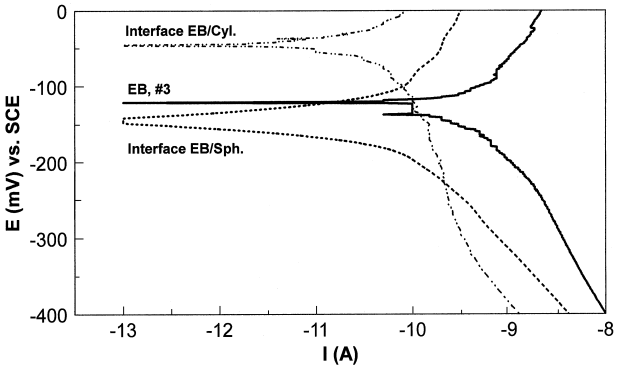

Fig. 8. Means of the potentiodynamic polarization curves measured from sample #3; weld EB #3; interface weld EB/cylindrical part; weld EB/spherical part.

be divided into two or more oxidation or reduction reactions, and (2) there can be no net accumulation of electrical charges during an electrochemical reaction.

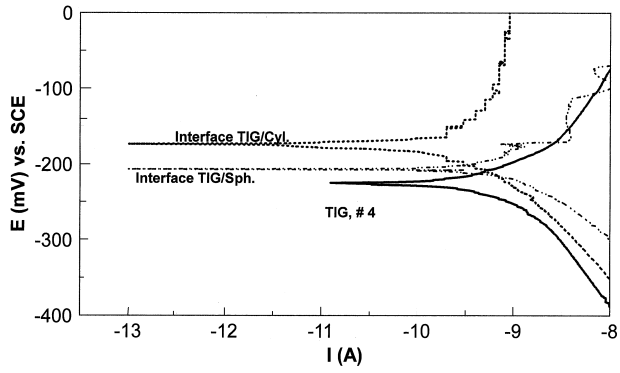

Fig. 9. Means of the potentiodynamic polarization curves measured from sample #4; weld TIG #4; interface weld TIG/cylindrical part; interface weld TIG/spherical part.

When two different corroding alloys are coupled electrically in the same electrolyte, both alloys are polarized so that each corrodes at a new rate [36]. If we apply the mixed potential theory, which consists of a practical method for obtaining the sum of the cathodic and anodic Tafel slopes of the welding and stainless steel couples studied, we obtain the predicted values E_{couple} and $I_{\text{corr couple}}$ culated couple potentials and currents are shown in a comparative manner in Table 4.

It appears that the $I_{\text{corr couple}}$ values are of the same order of magnitude (hundreds of picoamperes) as the values measured at the interfaces. The values calculated from the mixed potential theory are slightly higher than those measured from the polarization curves. The currents (I_{couple}) calculated from the mixed potential theory are also higher than those measured at the interfaces, and it confirms the better behavior of the EB type welds than those made with the TIG technique (Fig. 10).

The application of the mixed potential theory indicates that in sample #1, the weld EB #1 is in the cathodic position as compared to the stainless steel stem and sphere. However, welds in samples #2 and #4 are in the anodic position toward the stainless steel stem and sphere. The weld in sample #3 is cathodic toward the stainless steel sphere, and anodic toward the stainless steel stem. In Fig. 11, the relative anodic and cathodic positions of the materials at the interfaces are shown according to the mixed potential theory. The intercepts of the potentiodynamic polarization curves at the interfaces, with those in the welds (Figs. 6–9), lead to the same conclusion. As always, it is the anodic part which corrodes; since the welds are more sensitive to corrosion, it is preferable to choose a situation where the welds are in the cathodic position, as in sample #1. If the weld is in this cathodic position, the galvanic pile formed at the interface will not endanger the weld for other forms of corrosion (crevice, pitting, or intergranular corrosion) resulting from the galvanic coupling.

Table 4
Potential and coupling current (E_{couple}, I_{couple}): calculated according to the mixed potential theory. Comparison with values calculated from polarization curves measured at interfaces

Weld	Couple with cylindrical part				Couple with spherical part			
	#1, # 3		#2, #4		#1,#2		#3,#4	
	E_{couple} (mV)	I_{couple} (pA)	E_{couple} (mV)	I_{couple} (pA)	E_{couple} (mV)	I_{couple} (pA)	E_{couple} (mV)	I_{couple} (pA)
EB #1								
Predicted	+ 117	56	—	—	− 49	335	—	—
Measured	− 39	43	—	—	+ 21	169	—	—
EB #3								
Predicted	− 114	160	—	—	—	—	− 148	236
Measured	− 120	138	—	—	—	—	− 120	68
TIG #2								
Predicted	—	—	− 213	450	− 208	550	—	—
Measured	—	—	− 144	130	− 205	175	—	—
TIG #4								
Predicted	—	—	− 213	417	—	—	− 208	504
Measured	—	—	− 178	388	—	—	− 220	222

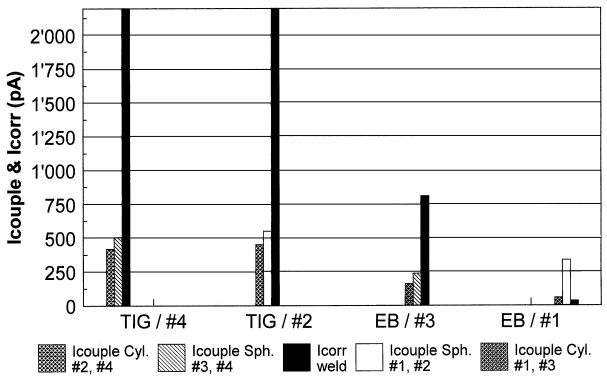

Fig. 10. Comparative presentation of the coupling currents calculated from the mixed potential theory, and of the measured corrosion currents of the welds.

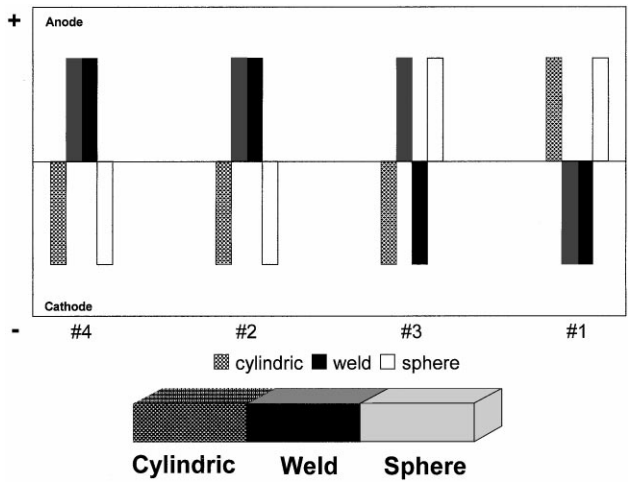

Fig. 11. Assessment of the cathode and anode in the galvanic couples tested according to the mixed potential theory.

3.2. Detecting susceptibility to intergranular attack

During the evaluation of the tested samples, particular attention has been paid to the behavior of the interface weld/stainless steel. Experience has shown that this zone is most prone to intergranular attack.

After the test for the intergranular corrosion, all samples have been observed at the interfaces, in the weld, and in the stainless steel stem and sphere, by optical microscopy (10 × enlargement) and by scanning electron microscopy (100 × enlargement).

The examination of these samples shows that in all non-sensitized samples, the welds do not exhibit intergranular attack. Analysis results of samples #2 and #3 are shown in Figs. 12 and 13.

Sensitized samples #1 and #4 do not show intergranular corrosion at the two interfaces of the weld with the two steels.

A sensitized sample #2 does not show any intergranular attack at the interface weld/stainless steel stem (Fig. 14); however, at the interface weld/stainless steel sphere, a zone of about 500 × 200 μm seems to exhibit some intergranular corrosion (Fig. 15). A higher enlargement of that zone is shown in Fig. 16.

A comparison of the EDX analyses performed in the core of a grain and at the grain boundary does not show any difference in the chemical composition. This seems to prove that there is no detectable dechromized zone

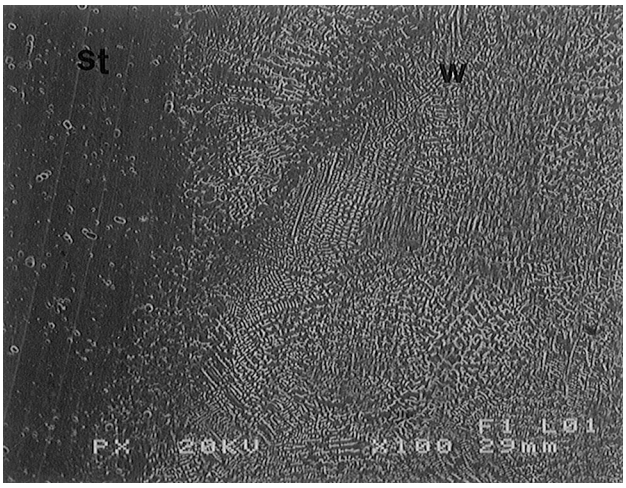

Fig. 12. Sample Code #2, non-sensitized TIG weld. Scanning electron microscopy 100×. Weld (w), stainless steel stem (st).

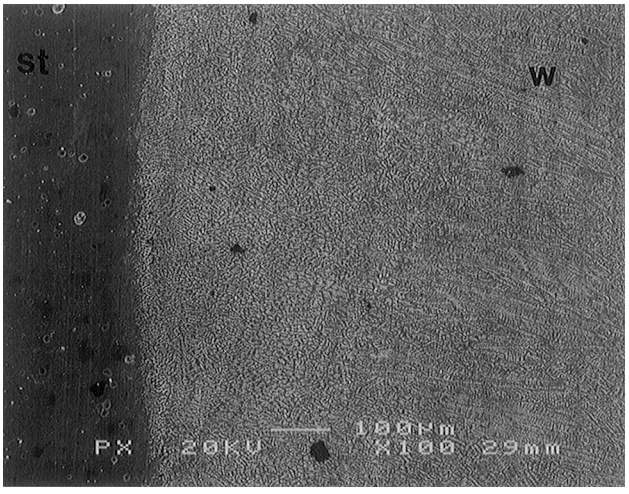

Fig. 13. Sample Code #3, non-sensitized EB weld. Scanning electron microscopy 100×. Weld (w), stainless steel stem (st).

Fig. 14. Sample Code #2, sensitized TIG weld (680°C, 1 h). Scanning electron microscopy 100×. Weld (w), stainless steel stem (st).

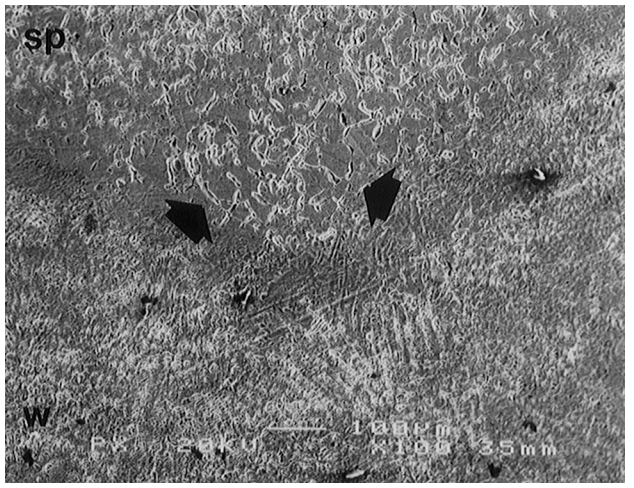

Fig. 15. Sample Code #2, sensitized TIG weld (680°C, 1 h). Scanning electron microscopy 100×. Weld (w), stainless steel sphere (sp). The marked area is shown enlarged in Fig. 18.

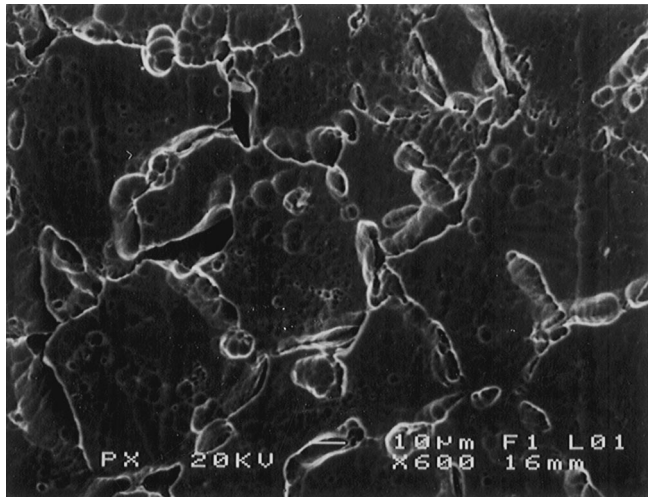

Fig. 16. Higher enlargement (600×) of the zone with the alleged intergranular corrosion at the interface weld/stainless steel sphere.

Table 5
Semi-quantitative EDX analysis in the zone of intergranular attack for material #2 (sensitized at 680°C for 1 h)

	Cr	Ni	Mn	Mo	Si	Fe
Surface	21.71	8.98	3.96	2.53	0.29	Balance
Grain boundary	21.70	9.24	3.99	2.18	0.30	Balance

(Table 5). According to Beaunier [37], intergranular corrosion can occur without dechromization (precipitation of chromium carbides); this is therefore an intergranular corrosion outside of precipitation. According to the same author, it is practically impossible to distinguish between

Fig. 17. Sample Code #3, sensitized EB weld (680°C, 1 h). Localized corrosion in the weld. 100×.

Fig. 18. Same welding zone as shown in sample Code #3, 1000×.

the influence of the atomic structure of a grain boundary, and that of the segregation.

Sample #3 (sensitized) shows some localized corrosion (pitting) in the weld, for a length of about 5 mm (Figs. 17 and 18).

The non-sensitized sample of the same orthopedic system combination (#3) does not present this type of degradation in the weld (see Fig. 13).

A summary of all the observations for the susceptibility to intergranular attack is presented in Table 6.

4. Conclusion

(a) Electrochemical evaluation:

- The measured corrosion currents I_{corr} and the predicted corrosion currents I_{couple} are low, in the range of pico- to nanoamperes. The predicted values I_{couple} are always higher than the measured ones.
- The welds of the type EB exhibit a better corrosion behavior than those of the TIG type.
- It is preferable that welds, which are corrosion-sensitive elements, are in the cathodic position. Therefore, the risk of starting localized degradations (pitting, crevice or intergranular corrosion) from the galvanic pile remains low. From this, sample #1 is better than the other tested samples, and combinations #2 and #4 give the worst results.
- No difference in the corrosion behavior has been observed among the two different mechanical treatments of the stainless steel used for the sphere (forged and forged and annealed).

(b) Evaluation of the susceptibility to intergranular attack:

- No particular corrosion has been observed at the interface weld/stainless steel on non-sensitized samples.

Table 6
Summary of observations on the resistance to intergranular corrosion

Welding	Code	Number of tested samples	Sensitized (680°C, 1 h)	Observations
TIG	#1	1	No	No corrosion at interfaces and in the weld
		2	Yes	No corrosion at interfaces and in the weld
	#2	1	No	No corrosion at interfaces and in the weld (cf. Fig. 12)
		2	Yes	One localized intergranular corrosion zone at interface weld/sphere (cf. Figs. 14–16)
EB	#3	1	No	No corrosion at interfaces and in the weld (cf. Fig. 13)
		2	Yes	Localized corrosion on the welding zone (cf. Figs. 17 and 18)
	#4	1	No	No corrosion at interfaces and in the weld
		2	Yes	No corrosion at interfaces and in the weld

- For sensitized samples, only sample #2 exhibits some localized intergranular corrosion on a short length (500 μm) of the interface weld/sphere.
- Sample #3 shows localized corrosion on some length (5 mm) of the welding.
- The materials, which exhibited some corrosion (#2 and #3), have nothing in common: welds and stainless steels used for the stem and the sphere are different (Table 2).

According to the results obtained in this study, there is no correlation between the various selected combinations for the assembly of the prosthetic elements studied, and their corrosion behavior. However, the corrosion tests performed with the microelectrode demonstrate a difference in the corrosion behavior of the welding systems used in the fabrication of the orthopedic prostheses: the EB welding system is clearly better than the TIG welding system. The electrochemical measuring technique used in this study has allowed a fine evaluation of the interfaces, which are the most corrosion-prone zones of the assemblies.

From the corrosion point of view, welding by electron beam (EB) seems therefore to be a viable method for joining implant parts made of REX 734 stainless steel, and should be preferred to the tungsten inert gas (TIG) welding technique.

References

[1] Kenneth FK. Corrosion of weldments. In: Metal handbook, vol. 13: Corrosion, 9th ed. ASM International, 1987. p. 344–68.

[2] Stricher MA. Intergranular. In: Baboian R, editor. Corrosion tests and standards. Application and interpretation. ASTM Manual Series, MNL 20, 1995. p. 197–224.

[3] Brown SA, Simpson JP. Crevice and fretting corrrosion of stainless-steel plates and screws. J Biomed Mater Res 1981;15: 867–78.

[4] Cook SD, Gerard PhD, Gianoli BS, Clemow AJT, Haddad PhD, Haddad RJ. Fretting corrrosion in orthopaedic alloys. Biomater Med Dev Artif Organs 1983–1984;11(4):281–92.

[5] Merritt K, Wortman RS, Millard M, Brwon SA. XPS analysis of 316 LVM corroded in serum and saline. Boimater Med Dev Artif Organs 1983;11(1):115–24.

[6] Merritt K, Brown SA. Effect of proteins and pH on fretting corrosion and metal ion release. J Biomed Mater Res 1988;22:111–20.

[7] Williams RL, Brown SA, Merrit K. Electrochemical studies on the influence of proteins on the corrosion of implant alloys. Biomaterials 1988;9:181–5.

[8] Fricker DC, Shivanath . Fretting corrosion studies of universal femoral head prostheses and cone taper spigots. Biomaterials 1990;11:495–500.

[9] Rieu J, Pichat A, Rabbe L-M. Ion implantation effects on friction and wear of joint prosthesis materials. Biomaterials 1991;12:139–43.

[10] Brown SA, Merrit K. Fretting corrosion in saline and serum. J Biomed Mater Res 1992;26:1131–9.

[11] Xulin S, Ito A, Tateishi T, Hoshino A. Fretting corrosion resistance and fretting corrosion product cytocompatibility of ferritic stainless steel. J Biomed Mater Res 1997;34:9–14.

[12] Duchyne P, De Meester P, Aernoudt E. Performance analysis of total hip prostheses: some particular metalurgical observations. J Biomed Mater Res 1980;14:31–40.

[13] Semlitsch M, Panic B. Corrosion fatigue testing of femoral head prostheses made of implant alloys of different fatigue resistance. In: Hastings GW, Williams DF, editors. Mechanical properties of biomaterials, vol. 2. New york: Wiley, 1980. p. 323–35.

[14] Smethurst E. A new stainlees steel alloy for surgical implants compared to 316 S12. Biomaterials 1981;2:116–9.

[15] Cahoon JR, Holte RN. Corrosion fatigue of sugical stainless steel in synthetic physiological solution. J Biomed Mater Res 1981;15:137–45.

[16] Bundy KJ, Vogelbaum MA, Desai VH. The influence of static stress on the corrosion behavior of 316L stainless steel in Ringer's solution. J Biomed Mater Res 1986;20:493–505.

[17] Taira M, Lautenschlager EP. In vitro fatigue of 316L col worked stainless steel. J Biomed Mater Res 1992;26:1131–9.

[18] Zabel DD, Brown S, Merritt K, Payer JH. AES analysis of stainless steel corroded in saline, in serum and in vivo. J Biomed Mater Res 1988;22:31–44.

[19] Harding AF, Cook SD, Thomas K, Collins CL, Haddad RJ, Milicic MG. A clinical and metalurgical analysis of retrieved Jewwet and Richards hip-plate devices. Clin Orthop 1985;195:261–9.

[20] Cook SD, Renz EA, Barrack RL, Thomas KA, Harding AF, Haddad RJ, Milicic M. Clinical and metallurgical examination of retrieved internal fixation devices. Clin Orthop 1985;194:236–47.

[21] Dorr LD, Bloebuam R, Emmanual J, Meldrum R. Histological, biochemical and ions anlysis of tissue and fluids retrieved during total hip arthroplasty. Clin Othop 1990;261:82–95.

[22] Walczak J, Shahgaldi F, Heatley F. In vivo corrosion of 316L stainless-steel hip implants: morphology and elemental compossition of corrosion products. Biomaterials 1998;19:229–37.

[23] Meachim G, Pedley RB. The tissue response at implant sites. In: Williams DF, editor. Fundamental aspects of biocompatibility, I. Boca Raton: CRC Press, 1981.

[24] Dobbs HS, Minski MJ. Metal ion release after total hip replacement. Biomaterials 1980;1:193–8.

[25] Thomas KA, Cook SD, Harding AF, Haddad Jr RJ. Tissue reaction to implant corrosion in 38 internal fixation devices. Orthopedics 1988;11:441–51.

[26] Brown SA, Flemming CA, Kawalec JS, Placko HE, Vassaux C, Merritt K, Payer JH, Kraay MJ. Fretting corrosion accelerates crevice corrosion of moduluar hip tapers. J Appl Biomater 1995;6:19–26.

[27] Jacobs JJ, Skipor AK, Doorn PF, Campbell P, Schmalzried TP, Black J, Amstutz HC. Cobalt and chromium concentrations in patients with metal on metal total hip replacements. Clin Orthop 1996;329 Suppl:256–63.

[28] Merritt K, Brown SA. Distribution of cobalt–chromium wear and corrosion products and biologic reactions. Clin Orthop 1996;329 Suppl:233–43.

[29] Jacobs JJ, Skipor AK, Patterson LM, Hallab NJ, Paprosky WG, Black J, Galante JO. Metal release in patients who have had a primary total hip arthroplasty. A prospective, controlled, longitudinal study. J Bone Jt Surg Am 1998;80:1447–58.

[30] Donati ME, Savarino L, Granchi D, Ciapetti G, Cervellati M, Rotini R, Pizzoferrato A. The effects of metal corrosion debris on immune system cells. Chir Organi Mov 1998;83:387–93.

[31] Suter T, Böhni H. Microelectrode methods for corrosion studies. 12th International Corrosion Congress, Huston, TX 3A, 1993. p. 1367–77.

[32] Suter T, Peter T, Bhöni H. Microelectrochemical investigation of MnS inclusions. Mater Sci Forum 1995;192–194:25–40.

[33] Suter T, Bhöni H. New microelectrochemical investigations to study the initiation mechanisms of ptting. In: Natishan PM, Kelly RG, Frankel GS, Newman RC, editors. Pro. Symp. Crit. Fact. Loc. Corr II, The Electrochemical Society Proceedings, vol. 95, 1996. p. 12–20.

[34] Standard practices for detecting susceptibility to intergranular attack in austenitic stainless steels, vol. 03.02. Philadelphia: American Society for Testing and Materials, 1991. p. 1–18.

[35] Wagner C, Traud W. Uber die deutung von korrosionsvorgängen durch überlagerung von elektrochemischen teillvorängen und über die potentialbildung an mischelektroden. Z Electrochem 1938;44:391–454.

[36] Baboian R. Electrochemical techniques for predicting galvanic corrosion. In: Baboian R, France Jr WD, Roew Lc, Rynewicz JF, editors. Galvanic and pitting corrosion-field and laboratory studies. ASTM STP 576, Philadelphia: ASTM, 1976. p. 6–19.

[37] Beaunier L. Corrosion intergranulaire hors précipitation. In: Corrosion Localisée. Les Ullis, France: Les Editions de Physique, 1994. p. 287–301.